IMPROVED CARRIER ACQUISITION IN 64QAM SYSTEMS

H. SARI and S. MORIDI

Laboratoires d'Electronique et de Physique Appliquée*
3, avenue Descartes, 94451 Limeil-Brévannes, France

ABSTRACT

Several phase and frequency detectors (PFD's) are presented for improved carrier acquisition in 64QAM systems. Some of them are based on rectangular signal representation, and form a direct extension to 64QAM of the PFD's previously proposed by the present authors for 16QAM systems. The others are new, and employ a phase detector based on polar-coordinate representation of the demodulated complex signal. A 34 Mbit/s laboratory breadboard was used to evaluate the performance of each detector. The best performance was obtained with the new PFD's derived from the polar phase detector. As compared with the original phase detector, these PFD's led to a 5- or 6-fold increase of the loop acquisition range.

INTRODUCTION

In some communication systems such as digital microwave radio links, the uncertainty and the drift of the oscillators typically result in large frequency offsets between the transmitter and the receiver. Consequently, the carrier recovery loop must be able to acquire lock over a large frequency range. On the other hand, the bandwidth-efficient modulation techniques used or considered for use in digital microwave radio, are very sensitive to carrier phase jitter, and require very narrow synchronization loops.

To meet these two requirements, the loop is usually designed with parameter values leading to sufficiently small noise bandwidth, and frequency-sweeping [1] is used to aid carrier acquisition. The acquisition problem is even more stringent in medium- and low-capacity links where the same absolute frequency offsets lead to larger normalized offsets (the normalization being made by the data rate). Note that, although very stable oscillators seem to be available [2], it is of considerable practical interest to design carrier recovery loops leading to a large acquisition range, and allowing the use of less stable and cheaper oscillators.

In a previous paper [3], some new phase and frequency detectors (PFD's) were proposed by the present authors, that form a very attractive alternative to frequency sweeping. They behave as a conventional phase detector (PD) in the steady-state, and as a frequency detector (FD) during acquisition. The result is a considerably large acquisition range while still meeting the stringent jitter requirements.

BASIC PRINCIPLE

The PFD's described in [3,4] are based on appropriate manipulation of a PD output. Specifically, given a discrete-time PD, its output is enabled when the instantaneous phase error falls within a predetermined interval $(-\Theta , +\Theta)$, and the last value is held in memory and used as the current input to the loop filter, otherwise. A general block diagram of decision-feedback carrier recovery loops employing this principle is depicted in figure 1. The discrete PD output is fed to a flip-flop whose clock is delivered by a digital control circuit that cancels the transitions of the symbol timing clock when the phase error lies outside the predetermined interval. In this diagram, the PD output is assumed binary ; in general, the loop requires as many flip-flops as the number of bits in the PD output, and all of them will be controlled by the same clock.

The PD we used in our previous studies is the polarity-type PD whose output at time k is given by

$$\xi_k = \mathrm{sgn}(e_k^y)\ \mathrm{sgn}(x_k) - \mathrm{sgn}(e_k^x)\ \mathrm{sgn}(y_k)$$

where sgn(.) denotes the mathematical sign function, x_k and y_k are the I and the Q channel outputs, respectively, and e_k^x and e_k^y are the instantaneous error signals given by

$$e_k^x = x_k - \hat{a}_k$$

and

$$e_k^y = y_k - \hat{b}_k$$

$\hat{a}_k$ and $\hat{b}_k$ being the decisions made on the I and the Q channels, respectively.

Furthermore, some square-shaped windows

* A member of the Philips Research Organization

CH2538-7/88/0000-1026 $1.00 © 1988 IEEE

were placed around the diagonal signal points of the signal constellation, and the symbol timing clock was enabled only when the received signal point falls within one of these windows.

The resulting PFD's were adequate for use in QPSK and 16QAM systems. Our experimental results in 16QAM indicated an increase of the acquisition range by more than an order of magnitude, using this strategy. Direct extension of this method to 64QAM, as initially suggested in [3], is illustrated in figure 2. Only 12 diagonal points of the signal constellation are used in these PFD's. The square windows placed around these points were all of the same size, leading to different values of the phase angle Θ . The resulting FD characteristics are given in figure 3, where the λ parameter determines the windows through the relations $|e_k^X| < \lambda$ and $|e_k^Y| < \lambda$. The frequency scale in this figure is normalized by the symbol rate 1/T. Smaller windows lead to higher FD gain for small frequency offsets, but what is most significant is the frequency range over which the FD output has the correct sign, and this is increased by making the windows larger. However, the PD used requires that the size of the windows be limited to the data decision boundaries. To choose larger phase angles, identical for all signal states, a modification of the PD was required. The experiments conducted using this PD showed only a moderate increase of the acquisition range that was deemed not sufficient to meet our objectives.

THE NEW DETECTORS

The polarity-type PD described in the previous section is based on rectangular signal representation. It is universal in that it can be applied to any digital modulation scheme, and is also simple to implement. However, other PD's may be more adequate for multilevel QAM signals. The PD described in [5] , and based on polar-coordinate representation of the demodulated complex signal, is particularly attractive for two reasons :

- first, it avoids false (phase-) lock phenomena (the PD characteristic has the correct sign over the whole period of the phase error),
- second, at equal peak values, it leads to a higher surface of the PDC, and consequently to a larger acquisition range (at least at high SNR's) as compared with the polarity-type PD based on rectangular signal representation.

We have developed new PFD's for 64QAM signals by combining this type of PD with our previously described method. A considerable improvement of the acquisition range has been achieved over the PFD's derived from PD's that are based on rectangular signal representation. This is primarily due to the fact that with this PD, the phase error interval ($-\Theta$, $+\Theta$) can be chosen arbitrarily for all of the signal points used in phase error estimation. Figure 4 shows, in a quadriplane of the signal constellation, the sign of the PD output as well as window choices for two PFD's, the first corresponding to an angle $\Theta = 10°$ and the second to $\Theta = 20°$. The first detector employs the hatched angular windows, and the second detector additionally employs the dotted windows, thus increasing the value of Θ from 10° to 20°.

Another PFD, derived from the same PD, and corresponding to an angle $\Theta = 30°$, is illustrated in figure 5. Again, only one quadrant of the signal constellation is shown due to the $\pi/2$-symmetry. Notice that, in addition to the windows around the diagonal points (d, d), (3d, 3d) and (7d, 7d), this PFD also employs some windows neighboring the signal points (d, 5d), (5d, d), (5d, 7d) and (7d, 5d). The reason for including the latter windows is the following :

As explained in [3,4], only the initially considered 12 diagonal points of the 64QAM signal constellation allow to determine the correct sign of the instantaneous phase error (mod. $\pi/2$) for every point on their trajectories during sync loss. For other points of the signal constellation, this is not strictly true, because the minimum angle between adjacent points on one circle is smaller than $\pi/2$. However, it can be easily verified that when the demodulated signal point is within one of the windows neighboring the signal points (5d, 7d) and (7d, 5d), the sign of the phase error (mod. $\pi/2$) is determined with no ambiguity, whether the transmitted point is a (5d, 7d) and (7d, 5d). The same argument holds for the two windows neighboring the signal points (d, 5d) and (5d, d). The three detectors presented in this section are referred to, in the sequel, as PFD1, PFD2 and PFD3, respectively.

EXPERIMENTAL RESULTS

A 34 Mbit/s 64QAM modem was used to evaluate the performance of the presented PFD's. In this modem, the demodulated I and Q signals enter an 8-bit A/D converter before driving the threshold detector. The dynamic range of the converters was limited to (-8, +8). The 6 most significant bits of the A/D converter output on both channels are used to address a read-only memory (ROM) in which the characteristics of the various PD's and PFD's are stored. The carrier recovery loop is a second-order loop that comprises a phase lead-

and-lag loop filter with transfer function

$$F(s) = \frac{1 + \tau_2 s}{1 + \tau_1 s}$$

where τ_1 and τ_2 are the loop constants.

In a first step, we measured the FD characteristics of six PFD's, three based on rectangular signal representation, and three on angular signal representation. The first three are those the theoretical characteristics of which are reported in figure 2. Their measured FD characteristics are depicted in figure 6. It can be seen that none of these detectors lead to a useful frequency range significantly higher than ± 200 kHz. The worst detector is obviously the one that corresponds to $\lambda = 0.25$, i.e. to the smallest windows. Figure 7 shows the FD characteristics of the latter three PFD's based on angular signal representation. The useful frequency range with these detectors exceeds ± 600 kHz.

Next, we measured the (mean) acquisition time of the presented PFD's vs. the frequency offset between the transmitter and the receiver. The results are given in figure 8 for the first three PFD's as well as for the corresponding PD. The loop parameters used in this experiment are

W_L = 140 kHz (noise bandwidth),
ζ = 2 (damping factor),
$K_0 = 4.06 \times 10^6$ rad/s/V (VCO gain),

and correspond to a phase jitter root mean-square (RMS) value of 0.3°.

A first observation is that the best results are obtained with the PFD that employs the largest windows ($\lambda = 0.75$), and the worst performance with the PFD that employs the smallest windows ($\lambda = 0.25$). A second observation is that even with the best one of these detectors, the acquisition range is only ± 120 kHz (for an acquisition time of 100 ms).

Finally, figure 9 shows the acquisition time vs. frequency offset for the phase detector based on polar signal representation and the three PFD's derived from it. The loop time constants used in these measurements are the same as previously, but the loop gain was increased so as to have approximately the same phase jitter RMS value as in the PD based on rectangular signal representation. The results indicate an acquisition range of ± 25 kHz for the original PD, and a range exceeding ± 200 kHz for PFD2 which corresponds to $\Theta = 20°$. PFD1 and PFD3 had similar performance, and resulted in an acquisition range of approximately ± 160 kHz (again for an acquisition time of 100 ms. From these results, we see that the new PFD's are considerably superior to the previously proposed ones that are based on rectangular signal representation.

It should be noted here that for 140 Mbit/s systems, the reported frequency offsets must be multiplied by 4, and the acquisition times must be divided by 4. Therefore, the measurement results reported in figure 9 for PFD2 must read, for 140 Mbit/s systems, an acquisition range of ± 800 kHz for an acquisition time of 25 ms. Using other loop parameters, we were able to extend the loop acquisition range to more than ± 1 MHz (for 140 Mbit/s systems) while still meeting the jitter requirements.

The last point that should be mentioned here is that after acquisition is achieved with the presented PFD's, the control logic of figure 1 must be disabled, and a logic 1 set at its output so as to enable the PD output at each symbol interval. This allows to keep the phase jitter in the PFD's exactly the same as in the phase detector from which they are derived.

CONCLUSIONS

Several PFD's have been presented for improved carrier acquisition in 64QAM systems. Those based on rectangular signal representation were found to have a modest performance due to the limited range of the angle that is usable for the outer diagonal points. Considerably better performance was achieved with PFD's based on polar signal representation. The latter ones lead to a sufficiently large acquisition range for 64QAM digital microwave radio systems, and form an attractive alternative to frequency-sweeping that is conventionally used to aid carrier acquisition.

REFERENCES

1 W.C. Lindsey, "Synchronization systems in communications and control", Prentice-Hall, Englewood Cliffs, N.J., 1972.

2 Y. Nakamura et al., "256QAM modem for multicarrier 400 Mbit/s digital radio", IEEE J. Select. Areas Commun., vol. SAC-5, n° 3, pp. 329-335, April 1987.

3 H. Sari et al., "A new class of frequency detectors for carrier recovery in QAM systems", ICC'86 Conf. Rec., vol. 1, pp. 482-486, June 1986, Toronto.

4 H. Sari and S. Moridi, "New phase and frequency detectors for carrier recovery in PSK and QAM systems", to appear in IEEE Transactions on Communications

5 M.H.W. Hoffmann, "Carrier recovery for M-QAM signals", Proc. European Conf. Radio Relay Syst. (ECRR), pp. 247-253, November 1986, Munich.

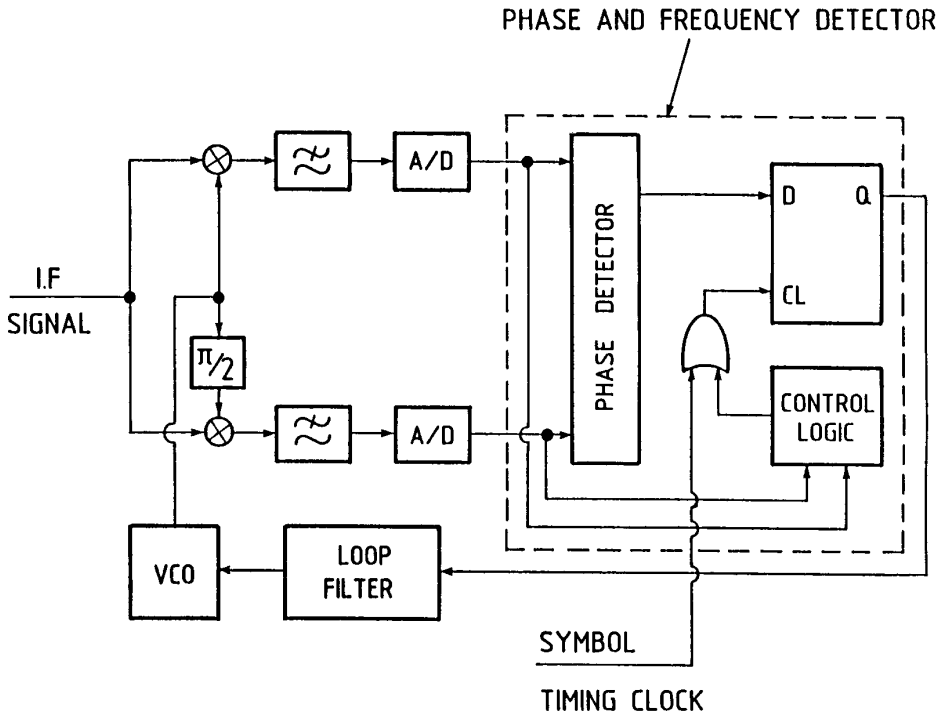

Fig. 1 : block diagram of a decision-feedback carrier recovery loop employing a PFD

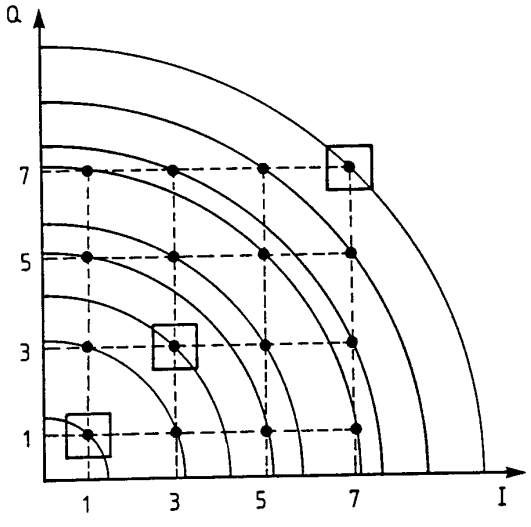

Fig. 2 : illustration (in one quadriplane) of a PFD based on rectangular signal representation ($\lambda = 0.5$)

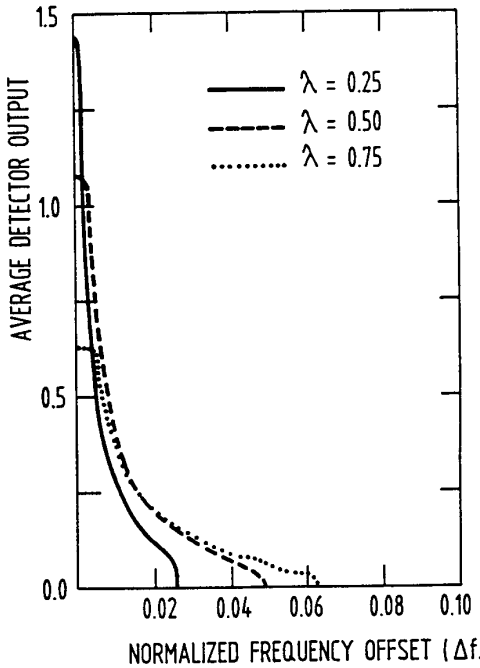

Fig. 3 : simulated FD characteristics of three PFD's based on rectangular signal representation

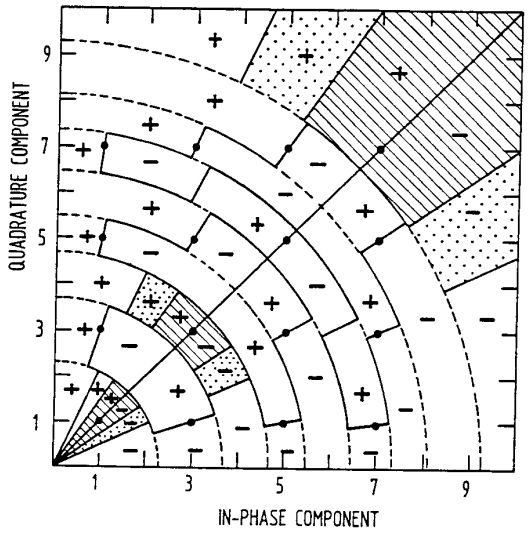

Fig. 4 : output of the PD based on polar signal representation, and window choices for two different PFD's, one corresponding to $\Theta = 10°$ and the other to $\Theta = 20°$

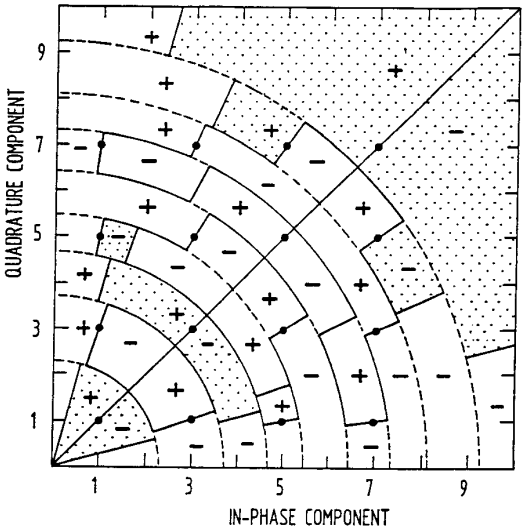

Fig. 5 : PD output and angular windows for the PFD corresponding to $\Theta = 30°$

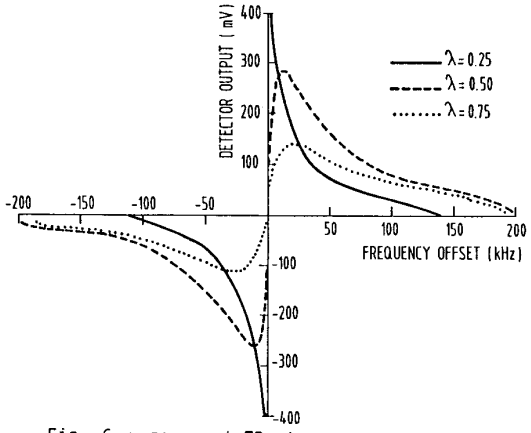

Fig. 6 : measured FD characteristics of the three PFD's based on rectangular signal representation

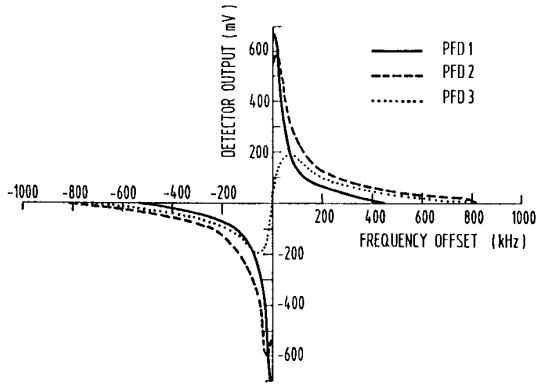

Fig. 7 : measured FD characteristics of PFD1, PFD2 and PFD3

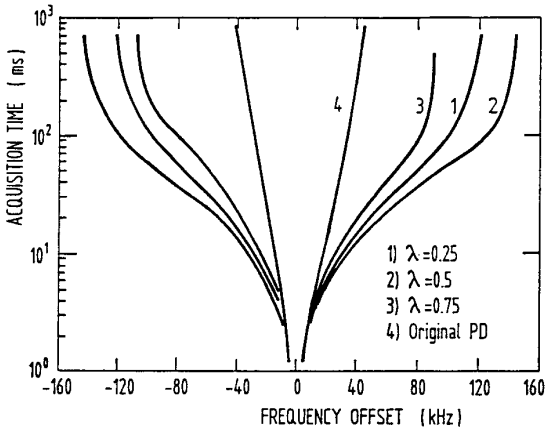

Fig. 8 : measured acquisition time vs. frequency offset with the three PFD's based on rectangular signal representation

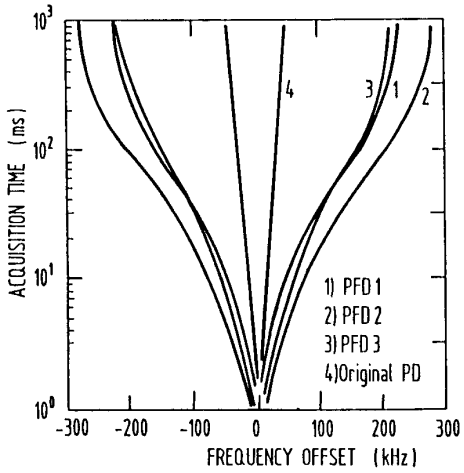

Fig. 9 : measured acquisition time vs. frequency offset witih PFD1, PFD2 and PFD3